

Ribbon-Ring 3D Design of the Metamaterial SRR Element

Vadym Slyusar

Central Research Institute of Armaments and Military
Equipment of Armed Forces of Ukraine
Kyiv, Ukraine
swadim@ukr.net

Ihor Sliusar

Department of information systems and technologies
Poltava State Agrarian University
Poltava, Ukraine
islyusar2007@ukr.net

Abstract— The paper proposes variants of 3D models of split ring resonators (SRR) based on ring structures as unit cells of doubly negative (DNG) metamaterials. Evaluation of the efficiency of the synthesized 3D SRR variants is based on determining their relative bandwidth, for which the real part of permittivity and permeability are negative. To analyze the electromagnetic properties of the proposed 3D SRR structures, numerical simulation in Ansys EM Suite was used. In the course of the research, an available set of geometric parameters that affect the width of the binegative zone in the low-frequency region of the spectrum was analyzed: the angles of deviation of the cuts in the rings from the vertical, the width of these cuts, variations in the cross-sectional dimensions of the perpendicular conductor and its displacement relative to the center of the rings. Non-traditional types of conductors were also studied, in particular options for the form in the form of a dumbbell and the use of a fractal tree. At the final stage of research, the main efforts were focused on the analysis of the influence on the frequency properties of the metamaterial unit cell model of the mutual displacement of the SRR rings relative to the middle of the conductor length and their inclination angles. As a result, the maximum relative frequency band of the binegative zone was reached, which is equal to 1.99995. This is superior to the previously obtained result for 3D SRR with square frames, for which this value corresponds to 1.9.

Keywords— double negative; metamaterial; split ring resonator

I. INTRODUCTION

An important direction in the development of Electrically Small Antennas (ESA) [1] for telecommunications and other applications is the use of metamaterials. Numerous publications on this topic have proposed various types of metamaterial elementary cell structures that make it possible to achieve certain values of characteristics that provide the solution to various problems of electrodynamics [2]–[13].

Among these works, the concept of 3D Split Ring Resonator (SRR) structures based on square split frames deserves attention [14]. In contrast to the classical prototype [15], the 3D square SRR models synthesized in [14] made it possible to expand the relative frequency band δf_{DNG} by approximately a factor of 10 (from 0.19 to ≈ 1.9), within which negative values of the relative permittivity and permeability simultaneously occur. ($\epsilon < 0$, $\mu < 0$) [2]–[5]. Such frequency bands will be further called double negative (Double Negative, DNG) according to the name of the corresponding metamaterials [2]–[5].

As is known [2]–[13], the use of metamaterials with binegative zones of values of the corresponding characteristics makes it possible to reduce the size of antenna radiators, expand their bandwidths, and increase radiation efficiency.

One of the important innovations in the 3D design of SRRs proposed in [14] was the orientation of a straight conductor in the direction perpendicular to the plane of placement of square frames. It was this solution that made it possible to expand the binegative zone in the low-frequency region. An additional novelty of the work [14] was given by the study of the influence on the characteristics of the metacell of the angles of deviation of the cuts of the SRR frames relative to the vertical axis within $0\div 90^\circ$. In addition, to expand the DNG frequency domain and simultaneously shift it down in frequency, it was proposed to use the mutual shift of the SRR frames relative to the rectangular conductor.

The improvements in the 3D topology of SRR considered in [14] are noteworthy in that they can be generalized to other variants of SRR design, in particular, based on round rings. At the same time, a sufficiently large degree of freedom in choosing the geometric parameters of 3D ring structures of this kind makes it relevant to study the corresponding dependencies and regularities in order to achieve the required parameters of the metacell design.

II. THE AIM OF RESEARCH

The aim of the work is to solve the problem of analyzing the properties of various variants of the 3D topology of metamaterial cells based on round ribbon SRR rings based on the results of electromagnetic modeling.

III. THE MAIN RESULTS OF THE STUDY

Before proceeding with the solution of the problem, it is necessary to determine the appropriate research methods. At the same time, it is essential to note that the complexity of the analytical description of the electrodynamics of 3D objects and, in particular, the set of components of the elementary cell of the metamaterial as a whole, makes it appropriate to give preference to choosing a possible option to achieve the goal of the study in favor of mathematical modeling.

As is known, the Ansys HFSS [15], [17], [18] and CST Studio Suite [19] packages are traditional and well-proven tools for modeling metamaterials. At the same time, the availability of access to the licensed version of Ansys HFSS within the Ansys EM Suite allows authors to limit

themselves to using this particular software ecosystem. In addition, as the practice of communicating with researchers on the ResearchGate forum has shown, CST Studio Suite does not accept negative values of permittivity.

In the case under consideration, the task is facilitated by the fact that Ansys HFSS already has a built-in macro for calculating the values of ε and μ , which is extremely important for identifying the DNG modes of functioning of metamaterial cells. The corresponding macro is based on the known relations [6]–[8]:

$$\mu = z \cdot n, \varepsilon = n / z, \quad (1)$$

where z is the wave impedance and n is the refractive index, calculated by the formulas [6]–[8]:

$$z = \sqrt{\frac{(1 + S_{11})^2 - S_{21}^2}{(1 - S_{11})^2 - S_{21}^2}} \quad (2)$$

$$n = \frac{1}{k_0 d} \arccos \left[\frac{1}{2S_{21}} (1 - S_{11}^2 - S_{21}^2) \right] \quad (3)$$

S_{xy} – S-parameters scattering matrix, $k_0 = 2\pi f/c$, d – the maximum linear size of a unit cell of a metamaterial, f – frequency of electromagnetic radiation, c – speed of light in a vacuum.

Another important factor in favor of choosing Ansys HFSS is the ability to discretely change the frequency of calculations linearly with a given step, while the available version of CST Studio Suite (Student Edition) uses the “sweep” mode by a given number of points on the frequency axis. This complicates obtaining in CST Studio Suite a sufficient accuracy of estimates of the properties of a metastructure elementary cell.

The next step in choosing the conditions and constraints for the simulation was to determine the boundary dimensions of the metacell and the corresponding air box. In order to maintain continuity with previous studies and facilitate comparison of the obtained results with previous publications of the authors, it was decided to use the key geometric parameters of the SRR that took place in [14].

metamaterial cell, presented in Fig. 1. It consists of two nested tapes of different diameters, 4.5 mm wide and 1.5 mm thick each, with an inter-tape interval of 1.5 mm. In this case, the outer diameter of the outer ring is 24.5 mm and corresponds to the length of the square conductor. This conductor is oriented parallel to the plane of the rings, and the distance from the center of the cross-section of the conductor to the center of symmetry of the rings is 4 mm. The cross-section of the conductor has dimensions of 1.5 x 1.25 mm with the long side oriented vertically. The cuts in the rings are located on the Z axis, the width of all cuts is the same and equal to the thickness of the tape, while the cut in the outer ring is located at the top. As a source of electromagnetic radiation, a modification of wave ports, called Floquet Port [15], [17], [18], was used. As is known, in ports of this type, the Floquet harmonic is excited, which has zero indices (it is often called the fundamental harmonic), which is identical in structure to the incident wave, while harmonics of higher orders do not propagate. When choosing the location of the excitation ports in the model, it was taken into account that in order to ensure the correct calculation of the scattering S-parameters, the ports

should be sufficiently removed from the near fields induced on the SRR structure. In addition, to efficiently estimate the S-parameters, the wave ports are placed on the inner surface of the box that describes the boundary conditions. As such conditions, from among those provided by Ansys HFSS, their variety of the “Master/Slave” type was chosen. It is taken into account that the 3D SRR model in fig. 1 is a single fragment of the periodic lattice of elementary cells.

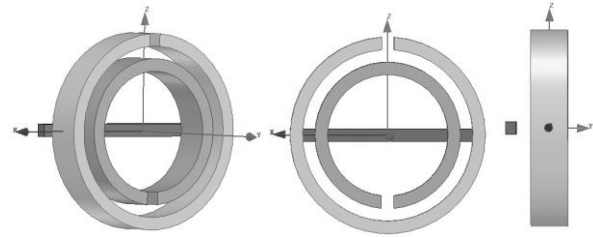


Fig. 1. The appearance of the 3D SRR model from different view angles.

Among the limitations adopted in the simulation, the following should be noted.

1. The frequency range involved in the calculation was in the range of 0.1÷10 GHz, although such an extensive segment was chosen only to obtain a complete picture, while the main attention was paid to the low-frequency region up to 1 GHz.

2. The SRR ring bands and the horizontal conductor were assumed to be made of copper.

3. The efficiency of the synthesized 3D SRR topology was evaluated by determining the relative frequency band for the metacell, within which the conditions of the binegative zone are satisfied [20]–[22]:

$$\delta f_{DNG} = \frac{2|f_1 - f_2|}{f_1 + f_2}, \quad (4)$$

where f_1 and f_2 are the boundaries of the frequency segment in which $\text{Re}(\varepsilon) < 0$ and $\text{Re}(\mu) < 0$.

4. The calculation mode was set to “Discret”, which allows you to get more accurate results.

Presented in Fig. 2, the results of calculating the real components of the quantities ε and μ indicate the presence of a binegative zone at low frequencies, extending from 100 to 442 MHz. This effect is very important for the implementation on the basis of the considered metacell of metamaterials for various purposes, which operate at wavelengths 15 or more times greater than the diameter of the outer SRR ring.

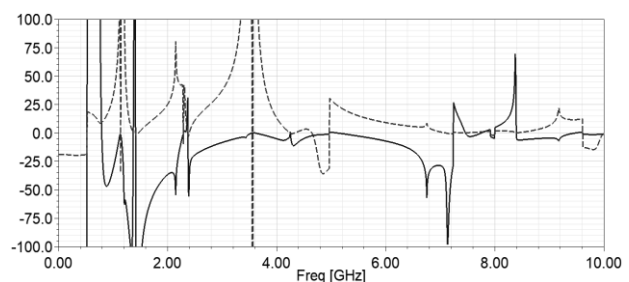


Fig. 2 Evaluation of the characteristics of the SRR model in fig. one, solid - $\text{Re}(\varepsilon)$; dash - $\text{Re}(\mu)$.

Further studies were aimed at analyzing the factors that affect the width of the low-frequency zone δf_{DNG} , as well as determining the geometric parameters of the metacell topology, which make it possible to expand this region to the maximum.

It should be noted that the presence of the region of interest in the frequency dependencies of the values of ϵ and μ is not observed for all orientations of the cuts in the rings relative to the Z axis. In particular, turning the cuts into a horizontal plane so that the axis passing through their centers is parallel to the conductor (Fig. 3) leads to the complete disappearance of the binegative zone at low frequencies (Fig. 4).

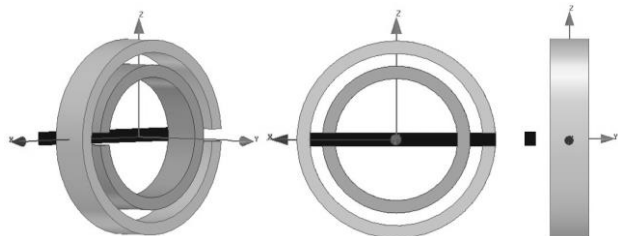


Fig. 3 SRR variant with horizontal cuts in the rings.

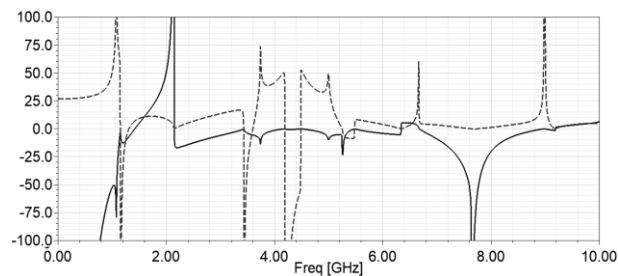


Fig. 4 Absence of a low-frequency binegative zone in the case of SRR with horizontal cuts in the rings: solid - $\text{Re}(\epsilon)$; dash - $\text{Re}(\mu)$.

A similar effect is also observed when the conductor is turned perpendicular to the plane of the rings (Fig. 5). In this case, the length of the conductor was set equal to 23.5 mm. At the same time, taking into account the efficiency of the transition in [14] to a perpendicularly oriented conductor, we will carry out further studies just for this case.

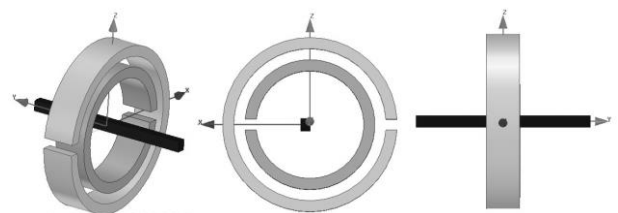


Fig. 5. SRR modification with perpendicular conductor arrangement.

Analyzing the set of geometric parameters available within the framework of the study under consideration, which are available for change, it should be noted that it is necessary to study the influence of the angles of deviation of the cuts in the rings from the vertical, the width of these cuts, as well as variations in the cross-sectional dimensions of the perpendicular conductor and its displacement relative to the center of the rings. The corresponding studies were carried out with a more detailed frequency sampling of 10 MHz, starting from the lower limit of 10 MHz and ending at 1 GHz. 1 GHz was also adopted as the decision frequency.

On Fig. 6 and 7 show selective results corresponding to a deviation of the center of the cuts in the rings from the vertical by 30° . The cross-sectional dimensions of the wire are 1.5 x 1.25 mm; In this case, the width of the low-frequency section of the binegative zone was 710 MHz. In terms of the relative bandwidth, this is an impressive value $\delta f_{DNG} = 1.9452$, which makes it possible to classify the synthesized metacell design as ultra-wideband.

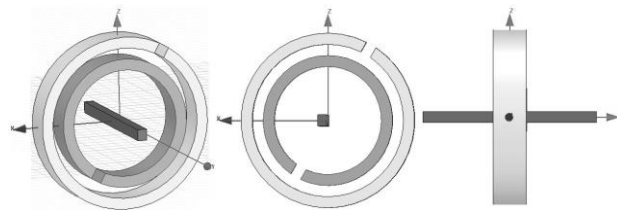


Fig. 6. SRR with a deviation of the center of the cut from the vertical by 30 degrees.

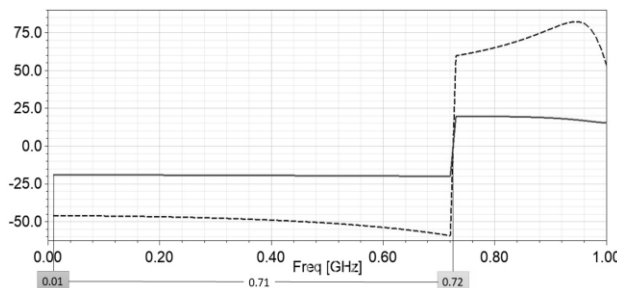


Fig. 7 The low-frequency binegative zone SRR in fig. 6: solid - $\text{Re}(\epsilon)$; dash - $\text{Re}(\mu)$.

Detailed values of the obtained frequency characteristics for other angles of inclination of the center of the cut in the outer ring are presented in Table 1. As follows from it, the best result in terms of the width of the strip in absolute terms is achieved in the case of deviations of the centers of the cuts from the vertical line by $60-70^\circ$. When passing to the relative values of the δf_{DNG} band, this corresponds to 1.9469. This effect slightly exceeds the result of [14], where $\delta f_{DNG} = 1.9$ was discussed. However, the fact that this gain was obtained at the very beginning of the research allows us to hope that it can be improved with further optimization of the parameters of the ribboning metacell.

One of the attempts to advance in this direction was to increase the width of the cuts in the tapes up to 3 mm. As it turned out, such a constructive solution made it possible to significantly expand the band of the binegative zone in the low-frequency region at zero deviation of the cut centers from the vertical z axis. In this case, instead of the interval 0.01 - 0.384 GHz, as indicated in Table. 1, the range of 0.01 - 0.684 GHz was obtained, which corresponds to $\delta f_{DNG} = 1.942$. Similarly, the upper limit of the low-frequency section of the DNG shifts to 0.71 GHz at a 20-degree deviation of the cut center from the vertical. At the same time, at angles greater than 30° , the effect of the expansion of the binegative zone is practically not noticeable. Thus, an increase in the cut width to 3 mm made it possible to significantly level out the differences in the DNG frequency band in the low-frequency region. Therefore, with further manipulations with other geometric parameters, it makes sense to fix the width of the cuts at the indicated level of 3 mm.

Following the plan outlined above, we analyze the

influence of the dimensions of the conductor cross-section. Corresponding dependencies of the $\text{Re}(\epsilon)$ and $\text{Re}(\mu)$ values for the angles of deviation of the cuts in the rings from the Z axis equal to 0 degrees, the width of the cuts 3 mm, and the wire cross-section 3 x 2.75 mm are shown in Fig. 8. As follows from the simulation results, the transition to a thickened conductor with its asymmetric position relative to the center of the rings did not lead to a narrowing of the low-frequency DNG band, the upper limit of which remained at around 684 MHz (Fig. 9).

TABLE I. DNG BANDWIDTH ESTIMATION FOR 1.5 MM CUTS

The angle of deviation of the center of the cut from the vertical, degrees	Cutoff frequencies, GHz		Bandwidth δf_{DNG}
	f_1	f_2	
0	0.01	0.384	1.898
10	0.01	0.724	1.9455
20	0.01	0.664	1.94
30	0.01	0.72	1.9452
40	0.01	0.724	1.9455
50	0.01	0.734	1.9462
60	0.01	0.744	1.9469
70	0.01	0.744	1.9469
80	0.015	0.804	1.597
90	-	-	-

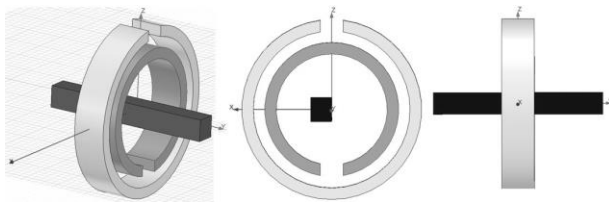


Fig. 8. SRR with 3 mm slots, 3 x 2.75 mm perpendicular conductor.

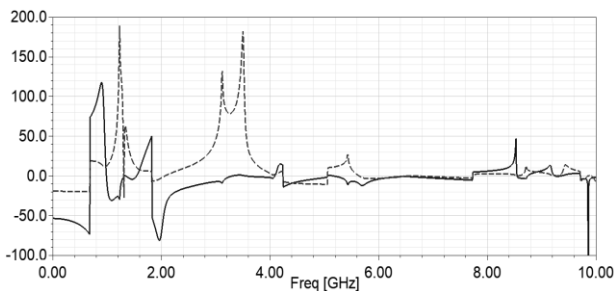


Fig. 9. Frequency dependencies of $\text{Re}(\epsilon)$ and $\text{Re}(\mu)$ for a metacell on fig. 8: solid - $\text{Re}(\epsilon)$; dash - $\text{Re}(\mu)$

The same result took place for other profiles of the conductor section, including the coincidence of the centers of the rings with the center of the conductor section (Fig. 10).

In the process of searching for solutions that expand the binegative zone at frequencies below 1 GHz, the design of a label cell with an unconventional conductor shape was also investigated. In particular, on Fig. 11 shows variants of a dumbbell-shaped conductor and the use of a fractal tree of various designs instead of it.

However, all these tricks did not allow expanding the band beyond the limits already indicated in Table. 1 indicator $\delta f_{DNG} = 1.9469$, although, for example, fractal trees provided local success in expanding the strip in the absence of deviation of the cut centers from the vertical axis.

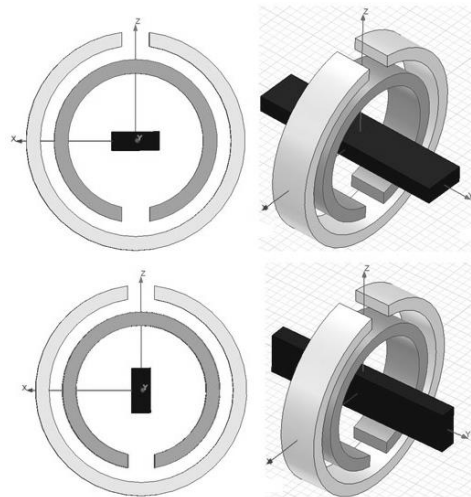


Fig. 10. Metacell variants with 2x5 mm (left) and 5x2 mm (right) conductors.

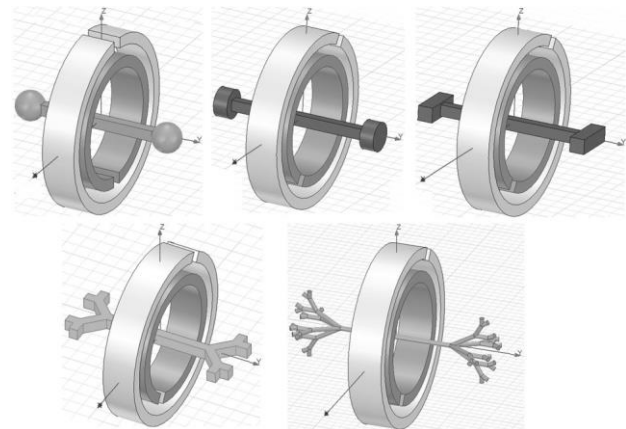


Fig. 11. Explored 3D SRRs with non-traditional conductors.

For example, the fractal tree shown at the bottom left in Fig. 11 provided the upper boundary of the binegative zone at a frequency of 697.4 MHz (the cuts in the tapes were 3 mm wide). The 3D design of the corresponding metacell is shown in Fig. 12.

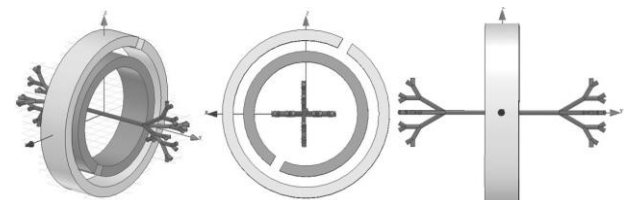


Fig. 12. A metacell with a fractal conductor provided a binegative range of 10 - 697.4 MHz.

Summing up the intermediate result of the work done, we can conclude that a more effective way to influence the width of the low-frequency binegative zone is to influence the geometric parameters of the ring-ribbon generators. This is explained by the fact that it is the tapes that are the first to contact the incident electromagnetic waves. Therefore, at the next stage of research, a variant of the metacell with different widths of the outer and inner ribbons was tested. In particular, in fig. 13 shows a variant of the metastructure with 3 mm cuts, a conductor cross-section of 1.5 x 1.25 mm, an outer tape width of 4.5 mm, and an inner tape width of 8 mm. At the same time, the DNG region of interest was localized within 10 - 680 MHz (Fig. 14).

Alternatively, when the upper bandwidth is 8 mm and the inner band is 4.5 mm (Fig. 15), the lower DNG band narrows to 430 MHz (Fig. 16).

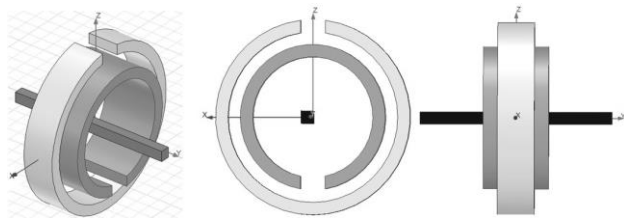


Fig. 13. Model with different belt widths.

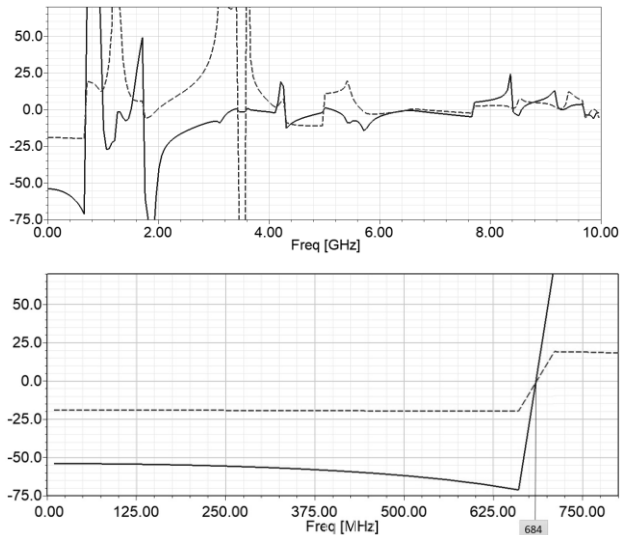


Fig. 14. DNG lower band increase to 680 MHz: solid - $\text{Re}(\epsilon)$; dash - $\text{Re}(\mu)$.

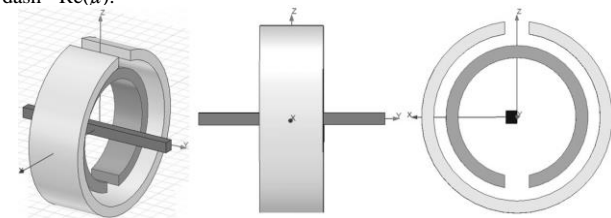


Fig. 15. Ribbon width combination alternative to fig. 12.

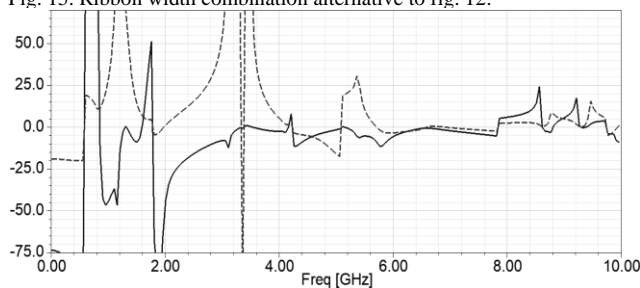


Fig. 16. Lower DNG Band Reduction to 430 MHz: solid - $\text{Re}(\epsilon)$; dash - $\text{Re}(\mu)$.

At the final stage of research, the main efforts were focused on the analysis of the influence on the frequency properties of the metamaterial unit cell model of the mutual displacement of SRR rings relative to the middle of the conductor length and their inclination angles along the Oz axis.

Taking into account the effect obtained in [14], the most detailed study was made of the SRR arrangement, which differed by the deviation of the ring planes relative

to the Oz axis by angles up to $\pm 45^\circ$ (Fig. 17). Since an increase in the specified angles can lead to a short circuit of the SRR rings, their opposite inclination was combined with the sliding of the rings relative to the middle of the conductor in order to avoid possible inter-ribbon contact.

The greatest indentation that could be achieved occurred at the angles of inclination of the rings $\pm 45^\circ$, their mutual displacement relative to the middle of the conductor ± 2.2 mm, a cut width of 3 mm, and conductor cross-sectional dimensions of 1.5×1.25 mm. As can be seen from Fig. 18, the lower DNG band in this case has expanded to 884 MHz, but the lower bound of the DNG zone jumped from 10 MHz to 35.5 MHz. This band corresponds to a value of $\delta f_{DNG} = 1.8456$. The price for such a value of δf_{DNG} was that the second binegative zone in the region of 4 - 5 GHz, characteristic of all the above-considered variants, in this case, crumbled into narrow sections.

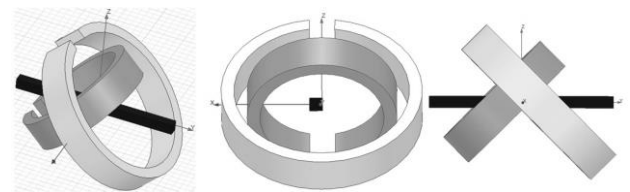


Fig. 17. SRR model with variations in the angles of inclination of the rings relative to the Oz axis.

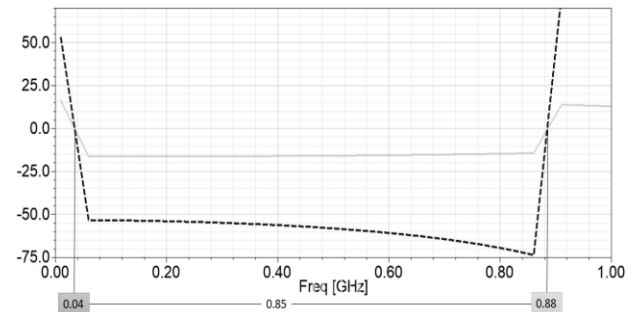


Fig. 18. Estimation of the frequency dependencies for SRR (Fig. 17): solid - $\text{Re}(\epsilon)$; dash - $\text{Re}(\mu)$.

In general, the considered 3D SRR models allow us to conclude that similarly to [14], the best width binegative zones in low-frequency regions are achieved by using both the mutual displacement of the SRR rings relative to the middle of the conductor and their opposite slope.

IV. PERSPECTIVESSING OF FURTHER RESEARCH

The authors plan to focus further research on the study of the electromagnetic properties of the considered SRR structures in the case of making ring tapes along a fractal structure [23], [24].

Another, no less interesting, direction in the development of the 3D design of ribbon-ring SRRs can be the integration of 3D square frames and round ribbon rings in one cell.

Since it is necessary to use the 3D printing process to build 3D SRR [25]–[28], an important direction for future research is to study the effect of printing defects and develop accuracy requirements for such technologies.

V. CONCLUSION

The paper presents the main results of studies of the electromagnetic properties of 3D tape-ring SRR structures, taking into account the influence of their key geometric parameters.

Compared to [14], the synthesized SRR models make it possible to obtain an additional increase in the value of δf_{DNG} from 1.9 to 1.9469.

The conclusion made in [14] was confirmed, that SRR with the conductor oriented perpendicular to the plane of the rings is an effective solution that guarantees the expansion of the binegative zone in the low-frequency region. To maximize it, it is also advisable to carry out the mutual displacement of the SRR rings relative to the middle of the conductor and tilt them towards each other within certain limits, excluding inter-tape closure.

REFERENCES

- [1] V. Slyusar, "60 Years of Electrically Small Antennas Theory", in *IEEE 2007 6th Int. Conf. on Antenna Theory and Techniques*, Sevastopol, 2007, pp. 116-118, DOI: <https://doi.org/10.1109/ICATT.2007.4425129>.
- [2] V. Veselago, "The Electrodynamics of Substances with Simultaneously Negative Values of ϵ and μ ," *Sov. Phys. Uspekhi* no. 10, pp. 509-514, 1968. DOI: <https://doi.org/10.1070/PU1968v010n04ABEH003699>.
- [3] V. Veselago, L. Braginsky, V. Shklover and C. Hafner, "Negative Refractive Index Materials," *Journal of Computational and Theoretical Nanoscience*, vol. 3, no. 2, pp. 189 - 218, April 2006. DOI: <https://doi.org/10.1166/jctn.2006.3000>.
- [4] V. Slyusar, "Metamaterials on antenna solutions," in *IEEE 2009 7th Int. Conf. on Antenna Theory and Techniques (ICATT'09)*, Lviv, 2009, pp. 19-24.
- [5] V. Slyusar, "Metamaterialy v antennoj tehnike: osnovnyye princypy i rezultaty" [Metamaterials in the antenna equipment: basic principles and results] *The First Mile (Pervaya milya)*, vol. 3, 4, pp. 44-60, 2010. (In Russian).
- [6] D. Smith, D. Vier, T. Koschny and C. Soukoulis, "Electromagnetic parameter retrieval from inhomogeneous metamaterials," *The American Physical Society. Physical Review E* 71, 036617 s2005d, DOI: <https://doi.org/10.1103/PhysRevE.71.036617>.
- [7] J. Pendry, A. Holden, D. Robbins and W. Stewart, "Magnetism from conductors and enhanced nonlinear phenomena," *IEEE Trans. Microw. Theory Tech.*, no. 47, pp. 2075-2081, 1999.
- [8] S. Nanda, D. De, P. Sahu and R. Mishra, "Metamaterial synthesis using a CAD model based on an evolutionary technique to improve the performance of TCAS antennas," *Journal of Computational Electronics*, vol. 18, pp. 1291-1305, 2019. DOI: <https://doi.org/10.1007/s10825-019-01367-7>.
- [9] S.S. Seetharaman, I.R. Hooper, and W.L. Barnes "Metamaterial Analogues of Molecular Aggregates Milo Baraclough", *ACS Photonics*, vol. 6 (11), pp. 3003-3009, 2019. DOI: <https://doi.org/10.1021/acsp Photonics.9b01208>.
- [10] J. Paul and A. Rekh, "Study and Analysis of Various SRR Patch Structures for Energy Harvesting Applications", in *2020 5th Int. Conf. on Communication and Electronics Systems (ICES)*, Coimbatore, 2020, pp. 326-329, DOI: <https://doi.org/10.1109/ICES48766.2020.9138062>.
- [11] M.-F. Wu et. al., "Miniaturization of a Patch Antenna with Dispersive Double Negative Medium Substrates," in *IEEE 2005 Asia-Pacific Conf. Microwave Proceedings (APMC 2005)*, China, [Online]. Available: <https://ieeexplore.ieee.org/document/1606177/authors#authors>.
- [12] C.T. Chevalier and J.D. Wilson "Frequency Bandwidth Optimization of Left-Handed Metamaterial", *NASA/TM-2004-213403*, November 2004. [Online]. Available: <https://ntrs.nasa.gov/archive/nasa/casi.ntrs.nasa.gov/20050019217.pdf>.
- [13] Z. Jaksic, M. Maksimovic and N. Dalarsson, "Negative Refractive Index Metamaterials: Principles and Applications," *Microwave Review*, pp. 36-49, Jun 2006.
- [14] I. Sliusar, V. Slyusar, Y. Utkin and O. Kopishynska, "Parametric synthesis of 3D structure of SRR element of the metamaterial," *2020 IEEE 7th Int. Sci.-Practical Conf. "Problems of Infocommunications. Science and Technology" (PICS&T'2020)*, Kharkiv, Ukraine, p. 6, 2020, DOI: <https://doi.org/10.1109/PICST51311.2020.9468067>.
- [15] S.E. Bankov, E.M. Gutzajt and A.A. Kurushin, *Reschenie opticheskikh i SVCH zadach s pomoshchyu HFSS [Solving optical and microwave problems using HFSS]* - Moscow, Russia: OOO "Orcada", 2012, 250 p. (In Russian).
- [16] K. Chand Ravi, V. Slyusar, J. Kumar, "SRR Loaded Wideband Antenna 5G Application," in *Second Int. Conf. on Artificial Intelligence and Signal Processing (AISP'22)*, Vijayawada, India, 2022, pp. 1 - 5. DOI: <https://doi.org/10.1109/AISP53593.2022.9760517>.
- [17] ANSYS HFSS. [Online]. Available: <http://www.ansys.com/Products/Simulation+Technology/Electronic s/Signal+Integrity/ANSYS+HFSS>.
- [18] S.E. Bankov and A.A. Kurushin, *Raschet antenn i SVCH struktur s pomoshchyu HFSS Ansoft [Calculation of antennas and microwave structures using HFSS Ansoft]*, Moscow, Russia: ZAO NPP "Rodnik", 2009, 736 p. (In Russian).
- [19] CST Studio Suite 2022 Student Edition. [Online]. Available: <https://www.3ds.com/products-services/simulia/products/cst-studio-suite/>.
- [20] Assessment of Ultra-Wideband (UWB) Technology. OSD/DARPA Ultra-Wideband Radar Review Panel, Battelle Tactical Technology Center, Contract No. DAAH01-88-C-0131, ARPA Order 6049. - July 13, 1990.
- [21] I. Sliusar, V. Slyusar, S. Voloshko and L. Degtyareva, "Antenna synthesis based on fractal approach and DRA technologies," in *IEEE 2th Ukraine Conf. on Electrical and Computer Engineering (UKRCON-2019)*, Lviv, 2019, pp. 29-34, DOI: <https://doi.org/10.1109/UKRCON.2019.8879953>.
- [22] I. Sliusar, V. Slyusar, S. Voloshko and V. Smolyar, "Synthesis of quasi-fractal hemispherical dielectric resonator antennas," in *IEEE 2018 5th Int. ScientificPractical Conf. Problems of Infocommunications. Science and Technology (PIC S&T)*, Kharkov, 2018, pp. 313-316, DOI: <https://doi.org/10.1109/INFOCOMMST.2018.8632087>.
- [23] I. Sliusar, V. Slyusar, S. Voloshko, A. Zinchenko and L. Degtyareva, "Synthesis of quasi-fractal ring antennas," in *IEEE 2019 6th Int. ScientificPractical Conf. Problems of Infocommunications. Science and Technology (PIC S&T)*, Kyiv, 2019, pp. 741-744, DOI: <https://doi.org/10.1109/PICST47496.2019.9061286>.
- [24] I. Sliusar, V. Slyusar, S. Voloshko, A. Zinchenko and Y. Utkin, "Synthesis of a Broadband Ring Antenna of a Two-Tape Design," in *2020 IEEE Ukrainian Microwave Week (UkrMW 2020)*, Kyiv, 2020, pp. 161-165.
- [25] C. Chen, C. Hsiao, S. Sun et al., "Fabrication of three dimensional split ring resonators by stress-driven assembly method," *Opt. Express*, vol. 20, Issue 9, pp. 9415-9420, 2012. DOI: <https://doi.org/10.1364/OE.20.009415>.
- [26] A. Salim, S. Ghosh, S. Lim, "Low-Cost and Lightweight 3D-Printed Split-Ring Resonator for Chemical Sensing Applications," *Sensors (Basel)*, 18(9):3049, 2018. DOI: <https://doi.org/10.3390/s18093049>.
- [27] A. Vallecchi, E. Shamomina and C. Stevens, "Analytical model of the fundamental mode of 3D square split ring resonators," *Journal of Applied Physics*, 125:014901, 2019. DOI: <https://doi.org/10.1063/1.5053482>.
- [28] Shengnan Li, Liuyang Zhang, and Xuefeng Chen. "3D-printed terahertz metamaterial absorber based on vertical split-ring resonator." *Journal of Applied Physics*, 130: 034504, 2021. DOI: <https://doi.org/10.1063/5.0056276>.